A Flow Analysis of the JAXA NEXST-1 using Hybrid Unstructured Grid System

Eiji Shima (shima_e@khi.co.jp) and Akio Ochi(ochi_a@khi.co.jp)

Kawasaki Heavy Industries, Ltd. (KHI)

ABSTRACT

This paper provides CFD flow analysis results of the JAXA NEXST-1 for the 4th JAXA SST CFD workshop. A hybrid unstructured grid system was employed for viscous aerodynamic analysis. Computations were conducted for the flight test condition, then computed and measured results are compared. Effects of some computational conditions, such as, choice of turbulence modeling, mesh density and numerical scheme, are studied.

Introduction

One of the major objectives of JAXA NEXT-1 is to serve high quality validation data to CFD. Force, pressure and some boundary layer characteristics at high Reynolds number and low turbulent flow without tunnel wall or support that cannot be achieved by wind tunnel test were obtained. CFD computations of the same conditions with the flight test are carried out and are compared with the experimental data in this study. In order to clarify the internal error of CFD effects of numerical scheme, mesh density and turbulence model are investigated.

Numerical Methods and Physical models

Hybrid Unstructured Grid System

The hybrid unstructured grid system used in this study consists of many hexahedral and prism cells with few pyramid and tetrahedron cells. Pyramid and tetrahedron cells are used as a link between hexahedral cells and prism cells. Surface grid consists of combination of quadrilaterals and triangles. Quadrilateral cell has a good property to obtain high resolution and high accuracy. Triangular cell is suitable for automatic surface mesh generation. In this study quadrilateral surface mesh is mainly used. The one of the benefit of this method is that rectangular mesh of high aspect ratio can be used for surface mesh. That enables the use of very small mesh size in chord-wise direction with keeping moderate mesh size in span-wise direction. (Fig.1)

Two meshes that have different number of layer is used in order to see the grid convergence.

Table-1 Number of cells in each mesh

Mesh	Fine	Coarse
Surface mesh	18289	18289
Volume mesh	1945536	1084809
Layer	141	83

Grid Generation

The hybrid grid in this study is generated by PUFGG (Pile-Up Forming Grid Generator) from surface grid. It automatically generates the volume grid starting from a surface grid and piles up layers as shown in Fig. 1. Near the body surface, hexahedral and prism cells will be created from quadrilateral and triangular surface cells. In the off body region, grid cells are merged in order to reduce the number of grid cells.

Flow Solver

The governing equations are the Thin layer approximated Reynolds averaged Navier-Stokes (RANS) equations.

An unstructured grid flow solver UG3, which is developed by the authors[1], is used for flow analysis. UG3 is based on unstructured FVM (Finite Volume Method). Spatial discretization is made by MUSCL (Monotone Upstream-centered Scheme for Conservation Laws). Two reconstruction methods for MUSCL are applied. Van Albada's differentiable limiter and its extension to triangular mesh are used in "2nd order methd" and Chakravarthy-Osher limiter and its extension are used in "3rd order method". Note that the latter scheme has 3rd order spatial accuracy in one dimension but true 3rd order accuracy can not be achieved by simple finite volume method in multi-dimension.

SHUS (Simple High-resolution Upwind Scheme)[2] is used to calculate the approximate Riemann fluxes. Time integration is performed by MFGS (Matrix Free Gauss-Seidel method).

Flow solver is parallelized by the means of domain decomposition and computations are carried out on PC cluster with 16 CPU cores.

RANS Turbulence Model

Spalart-Allmaras(SA) one equation turbulence model[4] is used as a standard in this study. Baldwin-Barth one equation turbulence model[5] is also applied for comparison.

The original SA model has transition term and stabilizing term for small disturbance. These terms are deleted in our computation. With this modification, SA model works in fully turbulent mode. Transition is controlled by turning off and on of the production source term in the boundary layer.

Finally the governing equation of SA model is written as follows,

$$\frac{D\tilde{\nu}}{Dt} =$$

$$c_{b1}\tilde{S}\tilde{\nu}f_{tr} + \frac{1}{\sigma}[\nabla\cdot((\nu+\tilde{\nu})\nabla\tilde{\nu}) + c_{b2}(\nabla\tilde{\nu})^2]$$

$$- c_{w1}f_w\left[\frac{\tilde{\nu}}{d}\right]^2$$

here f_{tr} is a newly introduced switch term to control transition and is mentioned in the next section.

Prediction of Laminar to Turbulent Transition

Prediction of laminar to turbulent transition is one of the most challenging problems in fluid dynamics and computational fluid dynamics. Even if e^N method is thought to be good enough for engineering use, it is not a simple problem to install it into unstructured RANS CFD solver in a robust way. The situation is similar to the use of algebraic turbulence models in unstructured grid CFD. As turbulence models themselves, algebraic models are simpler than one equation or two equation models, but use of latter are more straightforward in unstructured grid. Thus we follow similar way.

Very rough illustration of laminar to turbulent transition is growth of disturbance in the boundary layer. The growth of a turbulent variable in an one equation turbulence model, which directly related with turbulent viscosity, has qualitative similarity to the growth of physical disturbance. Thus one more equation for SA turbulence model in fully turbulent mode is computed simultaneously just for transition prediction. The boundary layer is judged to become turbulent when value of the maximum ratio of turbulent viscosity to molecular viscosity reach to prescribed threshold. The threshold value is adjusted through numerical experiment comparing with experimental data. 50 to 70 is appropriate value and 70 is selected in this study. Finally, equations to determine transition are written as follows.

$$\frac{D\tilde{\nu}_1}{Dt} =$$

$$c_{b1}\tilde{S}\tilde{\nu}_1 + \frac{1}{\sigma}[\nabla\cdot((\nu+\tilde{\nu}_1)\nabla\tilde{\nu}_1) + c_{b2}(\nabla\tilde{\nu}_1)^2]$$

$$- c_{w1}f_w\left[\frac{\tilde{\nu}_1}{d}\right]^2$$

$$\tilde{\nu}_{t1} = \frac{\chi^3}{\chi^3 + C_{v1}}\tilde{\nu}_1$$

$$f_{tr} = \frac{1}{2}\tanh\left\{\max_{B.L.}\left(\frac{\tilde{\nu}_{t1}}{\nu}\right) - Threshold\right\} + \frac{1}{2}$$

$$Threshold \approx 70$$

Configuration

The wing-body-tail configuration of AS(Aerodynamic Shape) of NEXT-1 defined by JAXA is used. The horizontal tail is fixed at zero degree and no aero-elastic effect is considered. Effects of horizontal tail angle are corrected on flight test data using wind tunnel test data.

Calculation condition

Following conditions that are same as pressure measurement points in the flight test are computed. Case A1 to A6 are called as 'Alpha sweep' and Case R1 to R9 are called as 'Reynolds number sweep'. (Table-2)

Used combinations of methods and mesh are summarized in Table-3.

Table-2 Flow conditions computed

Case	Mach	Incidence (deg)	Reynolds number (Million)
A1	1.9999	−1.5156	12.71
A2	2.0166	−0.0876	13.35
A3	2.0309	0.7666	14.23
A4	2.0206	1.5884	14.91
A5	1.9980	2.5395	15.51
A6	1.9682	3.4519	15.82
R1	1.9891	1.6952	33.98
R5	1.9491	1.6834	35.02
R9	1.8990	1.7079	34.68

Table-3 Combination of methods and mesh

Method	Turbulanece model	MUSCL	Mesh	Transition Prediction
1	SA	2nd	Fine	NO
2	SA	2nd	Fine	YES
3	BB	2nd	Fine	NO
4	SA	3rd	Fine	NO
5	SA	2nd	Coarse	NO
6	SA	3rd	Coarse	NO

Numerical Results and Discussion

3 component forces and effects of transition

The lift, drag and pitching moment coefficients of the flight test and by Method-1 and Method-2 are shown in Fig.4,5 and 6. The agreements of the lift and moment are fairly good, however they are not so good as comparison with wind tunnel test data.[3] Agreement of drag is improved by introducing the transition model. Although the crude transition model is used, effects of Reynolds number on transition are well estimated. Approximately 6 less drag count is calculated with transition prediction at lower Reynolds number.

Note that the threshold value in transition model is adjusted to give good agreement for low Reynolds number 'Alpha sweep' cases and same value is used for higher Reynolds number cases.

And note also that the additional drag on the flight test model by small measurement equipments that is computed as 6 drag count by other author's computation is not counted in this data. When this value is subtracted from the experimental data, difference become bigger.

Effects of scheme and mesh

Effects of numerical scheme, turbulence model and mesh are shown in Fig.6-9 by CD-CL characteristics of each case for fully turbulent flow. As shown in Fig.8-9, pressure forces agree within one drag count, thus most of differences come from viscous surface friction.

The agreement of cases using SA model are also quite good in spite of difference of mesh and spatial accuracy of the scheme. It indicates that present computation almost reaches to grid convergence solution.

The selection of turbulence model makes the most significant difference. BB model gives approximately 3 more drag count than the results by SA model.

Comparison of surface pressure

Comparisons of surface pressures computed by Method-1 and Method 2 with the flight test data are shown in Fig.10-12. Agreements are fairly good, however, significant difference that was not found in comparison with wind tunnel test data exist. There is no reasonable explanation to difference such as that on center body except for measurement error. The differences at wing tip shown in Fig.12 may due to aero-elastic effects.

Prediction of laminar to turbulent transition

Flight test measurement data for laminar to transition and iso-surfaces of turbulent viscosity in CFD for indicating turbulent are shown in Figure.

Agreement is generally good except for lower Reynolds number design point (Case A4). It is reasonable since that the crude transition model used in this study cannot predict effect of natural laminar flow design.

Conclusion

- It is shown that supersonic flow computation using 2 million cells in this study gives almost mesh converged solution.
- Since all pressure forces in the computations agree quite well, it can be said that accurate pressure force on rigid AS configuration is computed.
- BB turbulence model gives 3 count more drag than SA model.
- The simple estimation method for laminar to turbulent diverted from SA turbulence model works reasonably well.
- With transition estimation, 6 less drag count is calculated.
- Agreement of surface pressure with the flight test is fairly good, however, some difference that did not exist in comparison with wind tunnel test is found.

Acknowledgement

Geometry of NEXT-1, the flight test data and figures contains the flight test data is prepared by JAXA. The authors appreciate so much to their effort and cooperation.

References

[1] Shima,E., Ochi,A., Nakamura,T., Saito,S., Iwamiya,T., Unstructured Grid CFD on Numerical Wind Tunnel, in Parallel Computational Fluid Dynamics, pp.475-482, North Holland, (1999)

[2] Shima,E. and Jounouchi,T.," Role of CFD in Aeronautical Engineering(No.14) -AUSM type Upwind Schemes-", Proceedings of the 14th NAL Symposium on Aircraft Computational Aerodynamics, pp.7-1

[3] Ochi,A. and Shima,E., "A Flow Analysis of the NAL NEXST-1 using Hybrid Unstructured Grid System", Proceedings of Internal Workshop on Numerical Simulation Technology for Next Generation Supersonic Transport (3rd SST CFD Workshop), 03-05 December 2001, National Aerospace Laboratory of Japan, Tokyo, Japan

[4] Spalart, P. R. and Allmaras, S. R. "A one-equation turbulence model for aerodynamic flows", AIAA-92-0439, 1992

[5] Baldwin, B. and Barth, T., "A One-Equation Turbulent Transport Model for High Reynolds Number Wall-Bounded Flows," NASA TM 102847, 1990

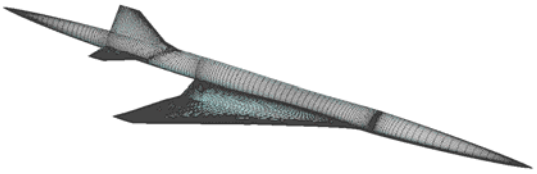

a) Surface grid

b) Inner middle layer

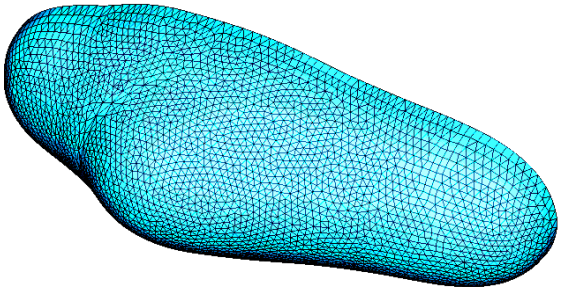

c) Outer middle layer

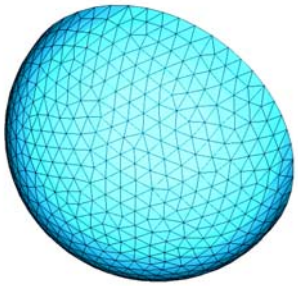

d) Outermost layer (1/20 scale)

Fig.1 Illustration of Growing volume grid.

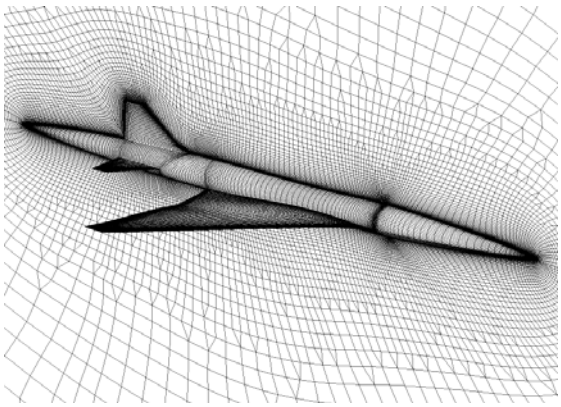

Fig.2 Surface and symmetry plane grid of NEXST-1

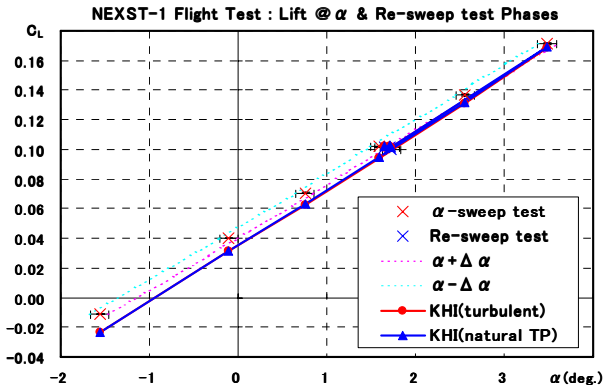

Fig.3 Lift coefficients of the flight test and CFD

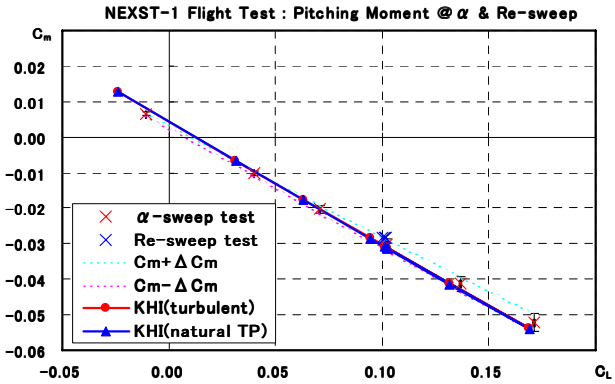

Fig.4 C_L-C_m of the flight test and CFD

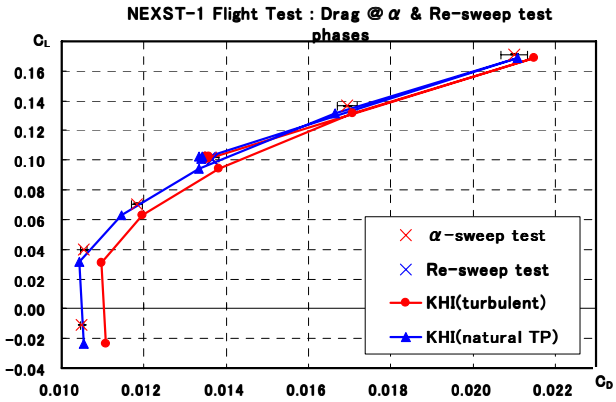

Fig.5 CD-CL of the flight test and CFD

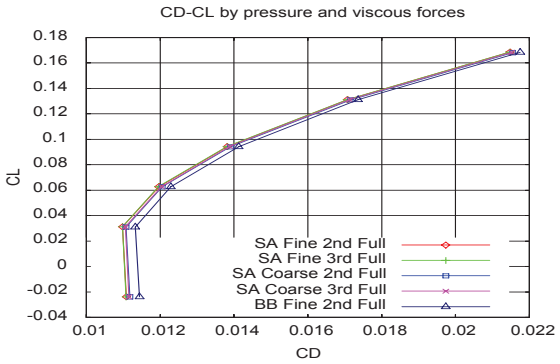

Fig.6 CD-CL of total force by each method

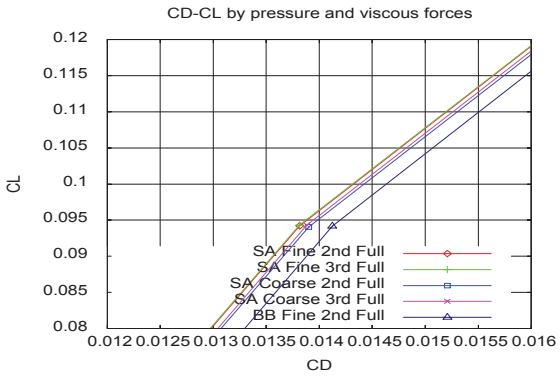

Fig.7 Enlarged view of CD-CL of total force by each method

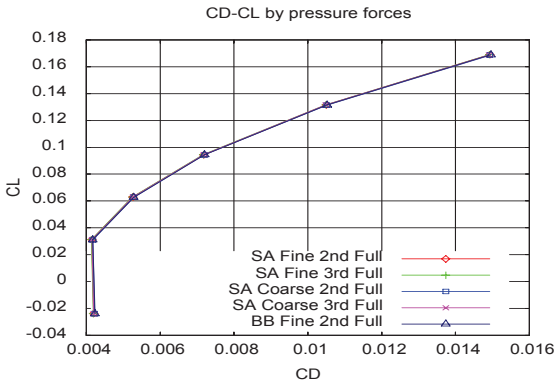

Fig.8 CD-CL of pressure force by each method

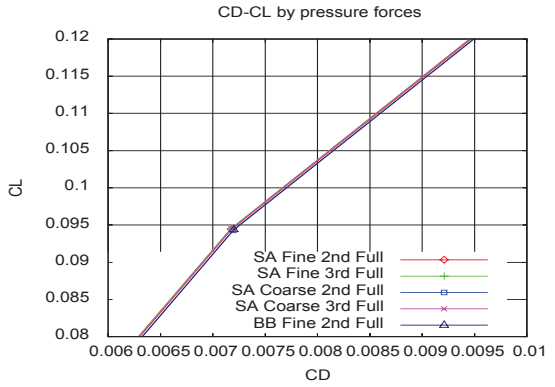

Fig.9 Enlarged view of CD-CL of pressure force by each method

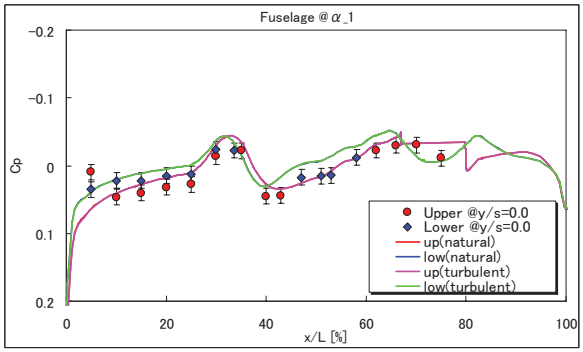

(a) A1

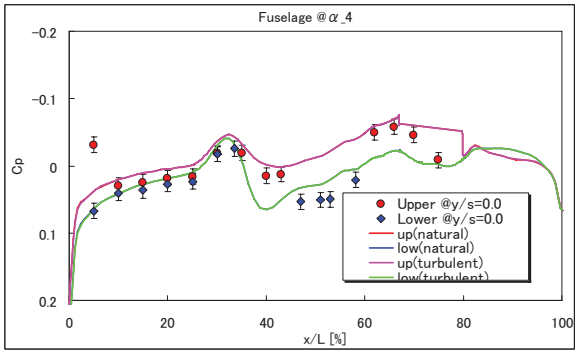

(b)A4

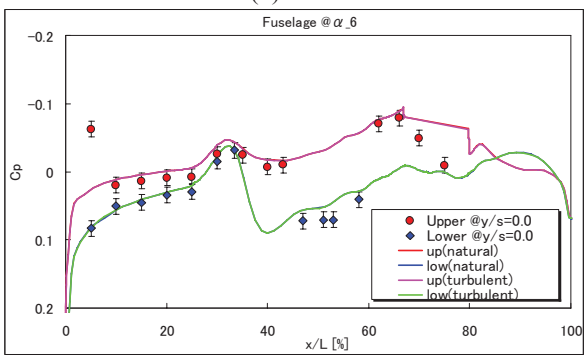

(c)A6

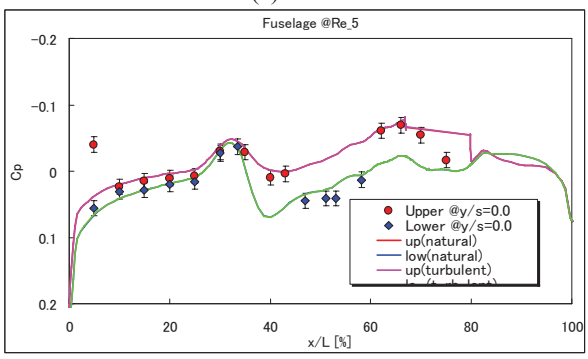

(d)R5

Fig.10 Pressure coefficients on the body center for case A1, A4, A6 and R5.

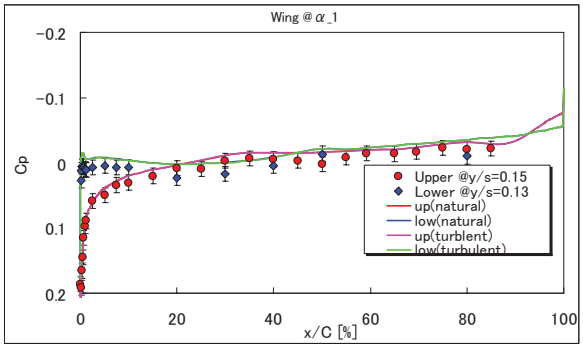

(a) A1

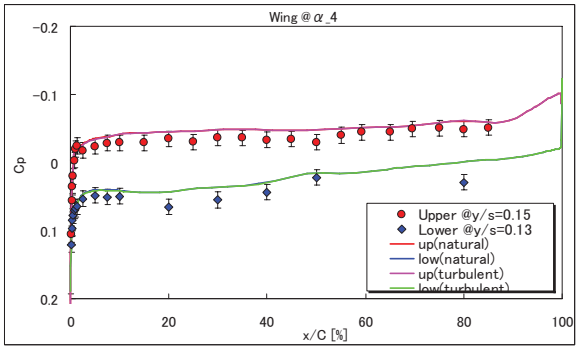

(b) A4

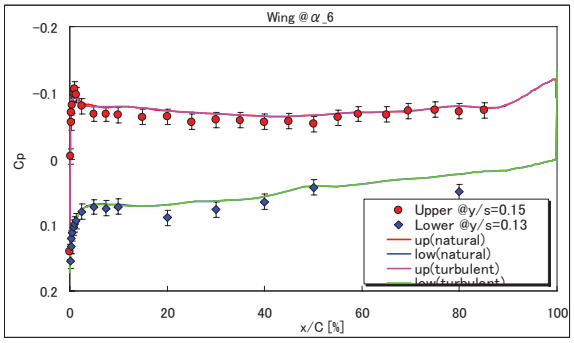

(c)A6

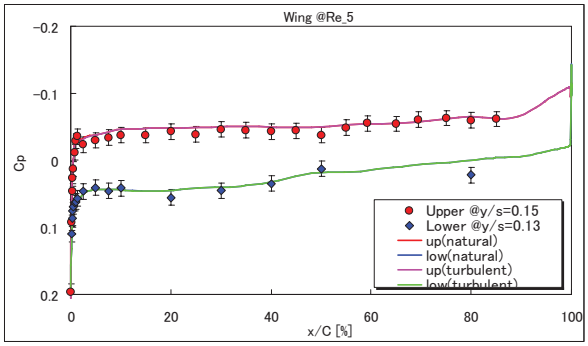

(d) R5

Fig.11 Pressure coefficients near wing root (at y/s=0.15) for case A1, A4, A6 and R5.

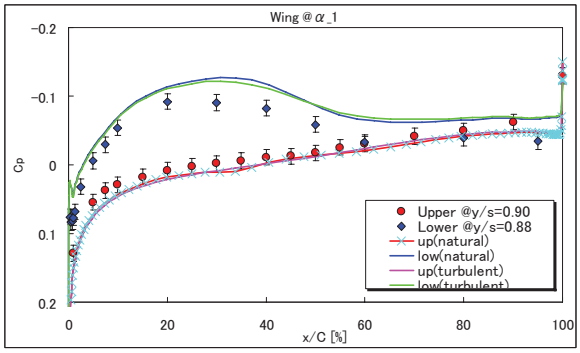

(a)A1

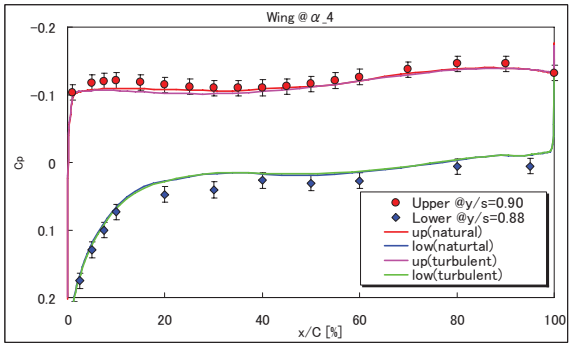

(b)A4

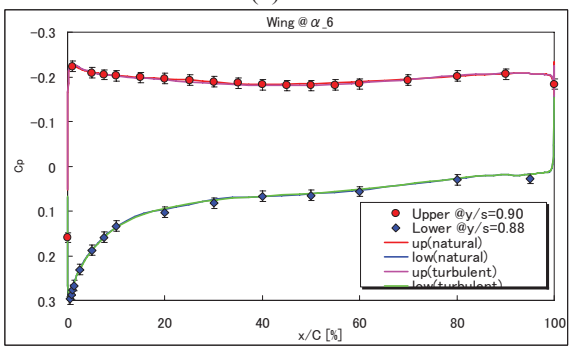

(c)A6

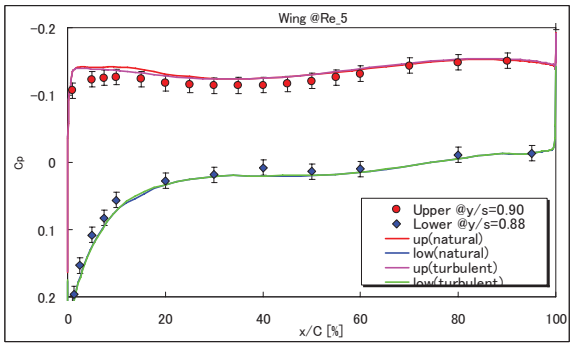

(c)R5

Fig.12 Pressure coefficients near wing tip (y/s=0.9) for case A1, A4, A6 and R5.

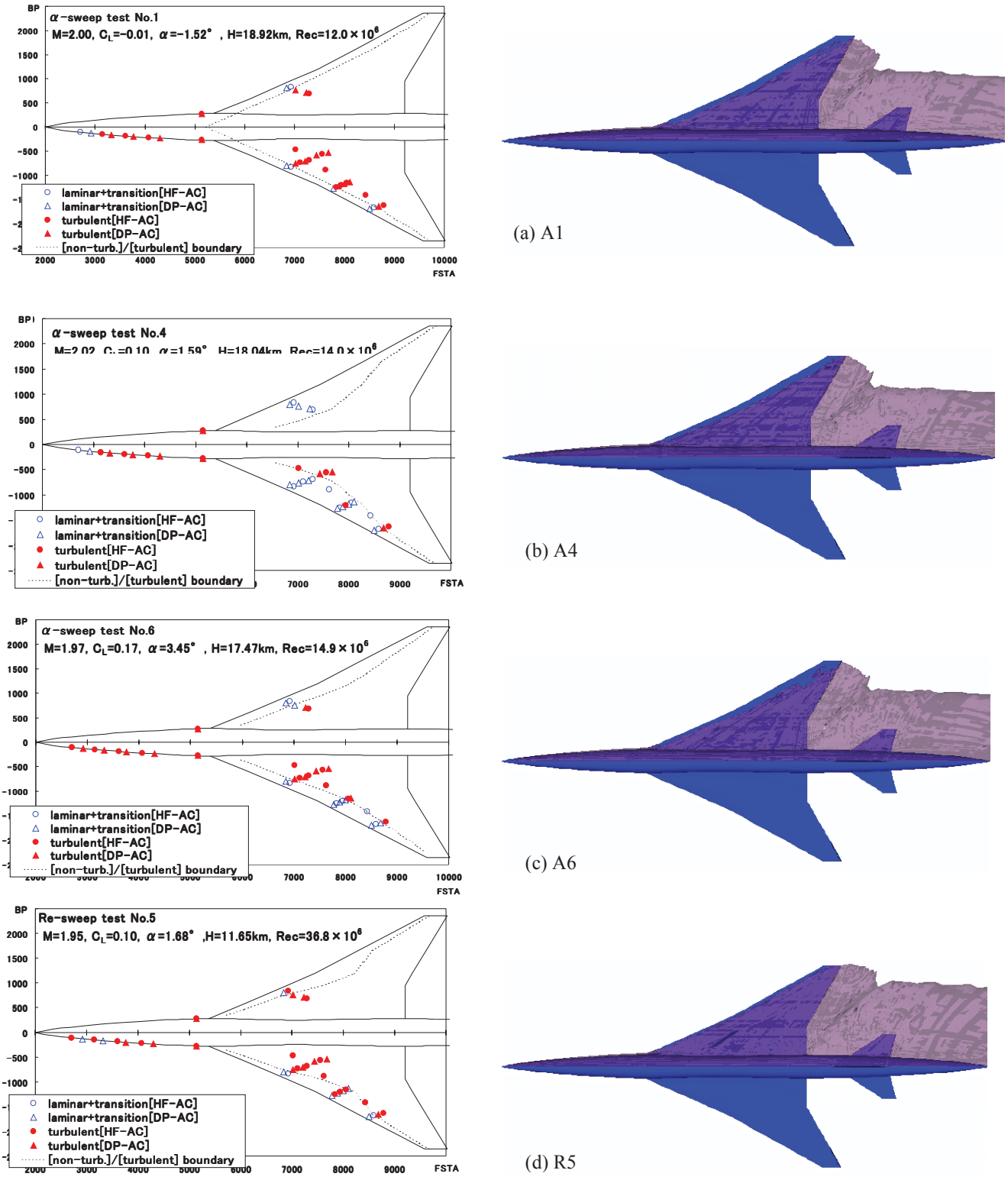

Fig.13 Transition measurements at the flight test (left) and iso-surfaces of turbulent viscosity (right) ,where ratio of turbulent viscosity to molecular viscosity is bigger than 10, are shown. Agreements are generally good except for Case-4 that is close to natural laminar design point in lower Reynolds number.